Fabrication of TiN-based Superhydrophobic Anti-corrosion Coating by Inverse Vulcanization

Congcong Miao,[1] Peiyao Yan,[2] Haichao Liu,[1] Shanshan (Diana) Cai,[2] Liam J. Dodd,[2] Haoran Wang,[2] Xi Deng,[2] Jian Li,[1] Xi-Cun Wang,[1] Xiaolin Hu,[3] Xiaofeng Wu,[1,2*] Tom Hasell,[1,2*] Zheng-Jun Quan[1*]

[1] College of Chemistry and Chemical Engineering, Gansu International Scientific and Technological Cooperation Base of Water-Retention Chemical Functional Material, Northwest Normal University, Lanzhou 730070, P.R. China

[2] Department of Chemistry, University of Liverpool, Liverpool, UK L69 7ZD

[3] Chongqing Key Laboratory of Green Energy Materials Technology and Systems, Department of Physics and Energy, Chongqing University of Technology, Chongqing, 40054, P.R. China

E-mail: xfwu@liverpool.ac.uk; T.Hasell@liverpool.ac.uk; quanzhengjun@hotmail.com.

Zhengjun Quan
Zhengjun Quan received PH.D. Degree from Northwest Normal University in 2007.
Zhengjun Quan worked as a visiting student at Technische Universität München in Germany from 2011 to 2012, his current research interests focus on the synthesis and application of sulfur-rich polymers as well as phosphine chemistry.

Abstract

Sulfur-rich polymers prepared by inverse vulcanization (IV), as a new chemistry and polymerization technique, have attracted increasing attentions since its' first invention in 2013. Although the extensive researches have been devoted into IV, there is still huge scope for advance, particularly, in terms of the practical applications of the resultant polymers. Previously SiO_2-embedded sulfur-rich polymers from IV were reported as superhydrophobic, antibacterial and anti-corrosion coating materials. We rreported herein the improved properties of superhydrophobic and anti-corrosion functional materials prepared by embedding more hydrophobic TiN nanoparticles into sulfur-rich polymers. This method provides fluoride-free composite materials, which is important considering the possible hazard to humans and the environment of concerns of fluorine-containing olefins with long carbon chains. Static water contact angles (WCA) of up to 173.6 ± 1.1° as well as superior properties such as higher superhydrophobicity and anti-corrosion (97.2% coating protection rate) are achieved. The generated coating has good to excellent self-cleaning functions. This protocol not only improves the superhydrophobicity of the synthesized composites, but also provides a feasible method for the preparation of non-harmful and environmentally benign fluorine-free superhydrophobic anti-corrosion materials applied in marine industries.

Keywords: Sulfur, superhydrophobic, anti-corrosion

1. Introduction

Sulfur is a by-product of petroleum and natural gas industry with extremely abundant storage extra to its consumable utilities, generating problematic environmental concern.[1] The low cost and high sulfur content of sulfur enable sulfur-rich polymers generated by inverse vulcanization (IV), a new chemistry and technology of copolymerization of sulfur with crosslinkers/monomers firstly demonstrated by Pyun and coworkers in 2013,[2] to exhibit unprecedented properties compared to their carbon-based counterparts. The unique nature and reactivity of S-S bonds in the resultant polymers motivates a wide range of multiple applications.[3,4] Due to the high sulfur content (from 50 to over 90 wt% in general) and the polysulfide structure of the polymer backbone, sulfur polymers have been found very interesting applications in many fields,[5-8] such as Li-S batteries,[9-11] metals recovery,[12-15] optical devices,[17,18] fertilizers[19,20] and antibacterial functions.[21-23]

Although extensive and various applications have been explored, practical applications of S-rich polymers produced by IV reaction are yet to be achieved, with more potential applications to be added. Therefore, it is of great significance to continuously contribute to the development of functionalized practical applications of these S-rich polymers. Thankfully to the nature of elemental sulfur,[23] the application of sulfur-rich polymers for antibacterial as well as anti-corrosive materials have been revealed to be feasible.[24-26] For example, materials as well as the coatings in the marine environment suffer from both corrosion and biofouling problems, and the adhesion of coatings is a key and crucial technology to improve the surface properties of materials for protection aiming for the extension of life time of their utilities and expansion of their application fields.[27] Coatings generally manifest as surface and interface problems between the coated membranes/films and the metal substrate, seawater and Cl^- penetrated into the coating and metal itself, resulting in corrosion of both coating and metal. Therefore, a superhydrophobic coating would be an ideal for effective approaches to reduce wettability of metal substrates by seawater and prevent corrosion.[28-30] Superhydrophobic surfaces are considered promising in various application fields such as self-cleaning,[31] oil-water separation,[32,33] water harvesting[34] and anti-corrosion.[35,36] Among those factors, the low surface energy and sufficient micro-nano roughness are the two critical factors to achieve superhydrophobicity.[37-39] Hong *et al.*[40] prepared a urethane-reactive coating material containing perfluoro-tert-butanol, and the polyurethane-coated fabric exhibited remarkable water repellency due to the umbrella-like structure

of perfluoro-tert-butanol and high water contact angle (WCA, 153°). We have previously demonstrated SiO_2-based fluorine-containing superhydrophobic antibacterial and anti-corrosion coatings derived from S-rich polymers via IV reaction with WCA of up to 154°, [41] however, there is still space to improve the performances of these coatings.

As a very special class of compounds, ionic liquids are easily coated on the surface of polar nanoparticles due to their large anionic and cationic dipole components. It has attracted much attention due to its antibacterial activity, low toxicity and good biocompatibility. Thus, replacing SiO_2 nanoparticles with TiN counterparts to gain more hydrophobic materials with micro-nano roughness may be beneficial. We presented herein our attempts to further improve the superhydrophobicity together with wettability of the coating by using ionic liquid cross-linking reagents: biimidazole ionic liquid crosslinker (VIMBr), S_8, and 1-octene (Octene) or perfluorooctene (PFO). This protocol provides fluoride-free composite coating with static WCA up to 173.6 ± 1.1° as well as anti-corrosion efficiency of over 97.2%.

Figure 1 shows the schematic diagram of the proposed preparation process and microstructures of TiN@Poly(S-VIMBr-Octene) (TiN@PSVO) or TiN@Poly(S-VIMBr-PFO) (TiN@PSVP).

2. Experimental

3.1 Synthesis of VIMBr

3,3'-(butane-1,4-diyl)bis(1-vinyl-1H-imidazol-3-ium) bromide (VIMBr) was synthesized according to literature (Figure S1).[42] In a 100 mL round-bottom flask equipped with a magnetic stirring bar and condenser, 1-vinylimidazole (4.00 g, 42.5 mmol) and 1,4-dibromobutane (4.75 g, 22 mmol) were dissolved into anhydrous methanol (50 mL), and refluxed at 70 °C for 48 h under argon atmosphere. After the reaction, the mixture was precipitated from diethyl ether (150 mL), and the solid was dissolved in methanol and precipitated from diethyl ether two times. The collected product was placed in a vacuum drying oven and dried at room temperature for 24 h to obtain a white solid biimidazolium bromide ionic liquid (VIMBr). Yield: 68.1%. ^{1}H NMR (400 MHz, D_2O), δ (TMS, ppm): 9.07 (s, 2H), 7.77 (s, 2H), 7.57 (s, 2H), 7.12 (dd, 2H), 5.79 (dt, 2H), 5.41 (dd, 2H), 4.29 (s, 4H), 1.95 (s, 4H). ^{13}C NMR (600 MHz, D_2O), δ(TMS, ppm): 134.18, 128.11, 122.63, 119.62, 109.48, 49.01, 26.00.

3.2 Synthesis of Poly(S-VIMBr-PFO)

To a 100 mL Schlenk tube equipped with a magnetic stir bar was sealed after the added S_8 (256 mg, 1 mmol) and $Zn(DTC)_2$ (12 mg, 1.5wt%), in which the air was cleared away using argon, connecting with the tail gas absorption tube to the branch of the Schlenk tube. When a yellow homogeneous solution was appeared at 135 °C from the mixture, VIMBr (404 mg, 1 mmol) was dissolved in methanol (1 mL), and DMF (9 mL) was injected into the mixture by syringe, following by a quick degassing with argon again. The mixture was then reacted for 5 h at the same temperature. After cooling down to room temperature, PFO (346 mg) in DMF (1 mL) was injected by syringe into the mixture with degassing and the resultant mixture was reacted for another 5 h at the same temperature. After cooling down, the mixture was precipitated in ethanol, filtered and washed with ethanol, and dried at 60 °C for direct use later, named as Poly(S-VIMBr-PFO), abbreviated as PSVP. In addition, PFO was replaced by 1-octene while other conditions were maintained, labeled as Poly(S-VIMBr-Octene), abbreviated as PSVO.

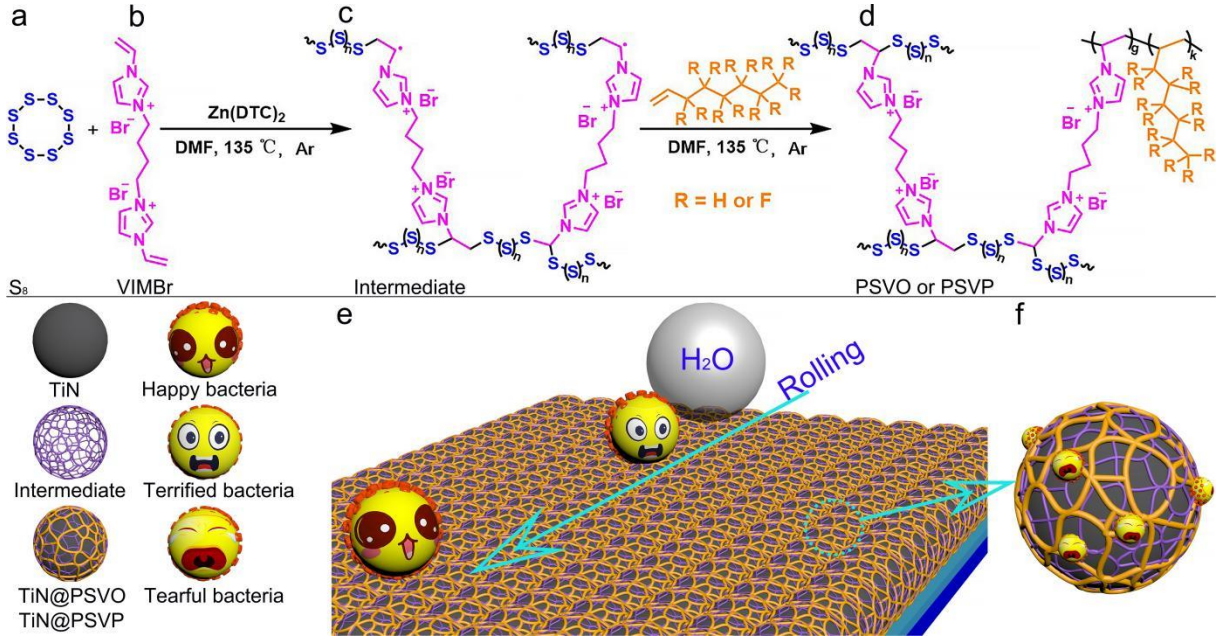

Figure 1. The proposed schematic diagram of TiN@PSVO or TiN@PSVP. S_8 (a), VIMBr (b), Intermediate (It is a proposed possible reaction intermediate, but unproven) (c), PSVO or PSVP (d), the proposed chemical reaction equations of PSVO or PSVP (d), water droplets roll away bacterium (e) and kill bacterium (f). The upper scheme represents the reaction process of S_8, VIMBr and 1-octene or PFO. The bottom of Figure 1 represents the coating materials as well as cartoon illustration of anti-corrosion process. Such as, TiN@PSVP sprayed on the substrate, the dark gray spheres represent TiN nanoparticles, and the purple and orange network structures represent the Poly(S-VIMBr) and PFO segments in TiN@PSVP, respectively. The blue arrows represent the rolling direction of the water droplets, the yellow balls with happy and terrified expressions represent the bacteria in different location of the coating surface, which should be brushed off by the water droplets; The yellow balls with crying expressions in (f) represent those bacterium are killed by quaternary ammonium salts on the coating surface.

3.3 Synthetic of TiN@Poly(S-VIMBr-PFO)

To a 100 mL Schlenk tube equipped with a magnetic stir bar was added TiN (30 mg) in DMF (8 mL), and the mixture was treated with ultrasonic for 30 min at 25 ℃. After the addition of S_8 (256 mg, 1 mmol) and $Zn(DTC)_2$ (12 mg, 1.5 wt%), the reaction tube was sealed and degassed thoroughly with argon, connecting with the tail gas absorption tube to the branch of the Schlenk tube. When a yellow homogeneous dispersed solution was appeared from the mixture with heating at 135 ℃, VIMBr (404 mg, 1 mmol) was dissolved in methanol (1 mL), and DMF (1 mL) was injected into the mixture by syringe, following by a quick degassing with argon again. The mixture was then reacted for 5 h at the same temperature. After cooling down to room temperature, PFO (346 mg, 1 mmol) in DMF (1 mL) was injected by syringe into the mixture with a quickly degassing with argon again and the resultant mixture was reacted for another 5 h at the same temperature. The obtained mixture was settled out with ethanol after cooling down, named as TiN@Poly(S-VIMBr-PFO), abbreviated as TiN@PSVP. In addition, various of the ratio of TiN applied for comparison while other conditions were maintained. Meanwhile, under the optimal ratio of TiN@PSVP, PFO was replaced by 1-octene, labeled as TiN@Poly(S-VIMBr-Octene), abbreviated as TiN@PSVO.

3.4 Self-cleaning experiment

The TiN@PSVP nanoparticles were sprayed on a glass slide, dried at 60 ℃ for 6 h without any further treatments, the resultant glass slide was tilted on a watch glass and sprinkled with a certain amount of sand. The water droplets were then dropped onto the coating surface to remove the sand, verifying the self-cleaning property of the coating. The self-cleaning performances of the coatings by water droplets were recorded by a digital camera.

3.5 Peeling test

The commercially available 3M 810 test tape was pasted onto the coating, and sufficient pressure was applied on the back of the test tape to make it completely adhere with the coating surface. The peeling test experiments were then carried out by quickly peeling off the tape from the coating surface, and following by a WCA measurement of the coating surface after sticking/peeling 5, 10, 50, 100 and 200 times.

3.6 Anti-corrosion experiment

AZ31B Mg (Mg) alloy (2.5 × 1.0 × 0.05 cm) polished with 400 grit sandpaper to remove the passivation layer on the surface, was ultrasonically cleaned in acetone and ethanol for 30 minutes, and then dried naturally in the air. The electrode of Mg was wrapped with tape except the targeted exposed test area (1 cm^2) around the bottom dipped in the electrolyte as well as the top connection point. The designed coating was prepared by the spraying the dispersed solution of TiN@PSVP and TiN@PSVO onto the Mg alloy and dried it in an oven at 60 ℃ for 6 h. A three-electrode electrochemical workstation system was adopted, the counter electrode is a platinum sheet, the reference electrode is silver/silver chloride (Ag/AgCl), the working electrode is bare Mg alloy or coated Mg alloy, and the electrolyte is composed of 3.5% NaCl aqueous solution. The Tafel curve at a rate of 10 mV/s of the exposed coating surface was then measured within -2 ~ 1 V range to clarify the anti-corrosion effect.

3.7 Antibacterial experiment

Antibacterial activity of TiN@PSVP nanoparticles were evaluated by the plate count method. Gram-positive *Staphylococcus aureus (S. aureus)* and Gram-negative *Escherichia coli (E. coli)* were selected as representative bacterial strains. Single colonies of *E. coli* and *S. aureus* strain were selected from the Luria-Bertani (LB) agar plate and inoculated in LB fluid nutrient medium (50 mL). Bacteria suspensions were grown under shaking (200 rpm) at 37 ℃ for 15 h. The suspensions were diluted by phosphate buffered saline (PBS) solution to acquire 10^6 CFU/mL bacteria samples. To evaluate the antibacterial properties of TiN@PSVP nanoparticles (10 mg, 200 μg/mL) were co-cultivated with bacteria, and the blank group, only the bacteria solution was added without the sample, and it was placed in a constant temperature shaking (200 rpm) at 37 ℃ for 6 h. After the culture was completed, PBS solution was used to dilute the culture solution continuously by 10 times, and then the resultant diluted solution (120 μL) was taken and spread evenly on the LB solid medium. The resultant plate was then placed in a constant temperature incubator at 37 ℃ for 18 h, observing and taking pictures to record the number of colonies. Each group was set up with 2 parallel repetitions. In addition, all samples and utensils in the experiment were sterilized in prior in a high-temperature and high-pressure steam sterilizer at 121 ℃ for 30 min.

3. Results and Discussion

Synthesis and Characterization of PSVP

Followed our previous study of achieving superhydrophobic materials with SiO_2-embedded S-rich polymers, the replacement of SiO_2 nanoparticles with more hydrophobic TiN counterparts was conducted with the optimized reaction conditions. As shown in Table 1, there are no considerable difference of WCA for the obtained new TiN-embedded S-rich polymers with the same crosslinkers, such as TiN@poly(S-DIB-octene), TiN@poly(S-DVB-Octene) and TiN@poly(S-DAS-Octene) (Entries 1-3 in Table 1, Figure S3-9); limited improvements were observed even with the low surface energy PFO (Entries 4-6 in Table 1, Figure S3-9).

Ionic liquids are easily coated on the surface of polar nanoparticles due to their large anionic and cationic dipole moments. The fluorine-containing polymers are much easier than fluorine-free polymers for the structural identification of the obtained materials. Thus, S-rich polymers were synthesized by

Table 1 Change the WCA influenced by different crosslinkers with octene or PFO.

Entry	S:C:PFO /mol	S /mmol	C[a] /mmol	Octene/PFO /mmol	WCA /°
TiN@Poly(S-DIB-Octene)	1:1:1	1	1	1	158.4±0.4
TiN@Poly(S-DVB-Octene)	1:1:1	1	1	1	162.6±1.6
TiN@Poly(S-DAS-Octene)	1:1:1	1	1	1	152.2±0.7
TiN@Poly(S-DIB-PFO)	1:1:1	1	1	1	165.4±0.7
TiN@Poly(S-DVB-PFO)	1:1:1	1	1	1	157.5±0.9
TiN@Poly(S-DAS-PFO)	1:1:1	1	1	1	166.8±0.3

a: C represents crosslinker

IV with S_8, VIMBr and PFO at the presence of $Zn(DTC)_2$ catalysts. After the reaction of S_8 (256 mg) with VIMBr (404 mg) in the presence of $Zn(DTC)_2$ (1.5 wt%) under inert atmosphere at 135 °C for 5 h reaction, PFO (346 mg) was added and the reaction was continued for another 5 h to obtain PSVP. The structure of the obtained PSVP was characterized with NMR and FTIR spectra. As shown in the ^{1}H NMR spectrum (Figure 2a),

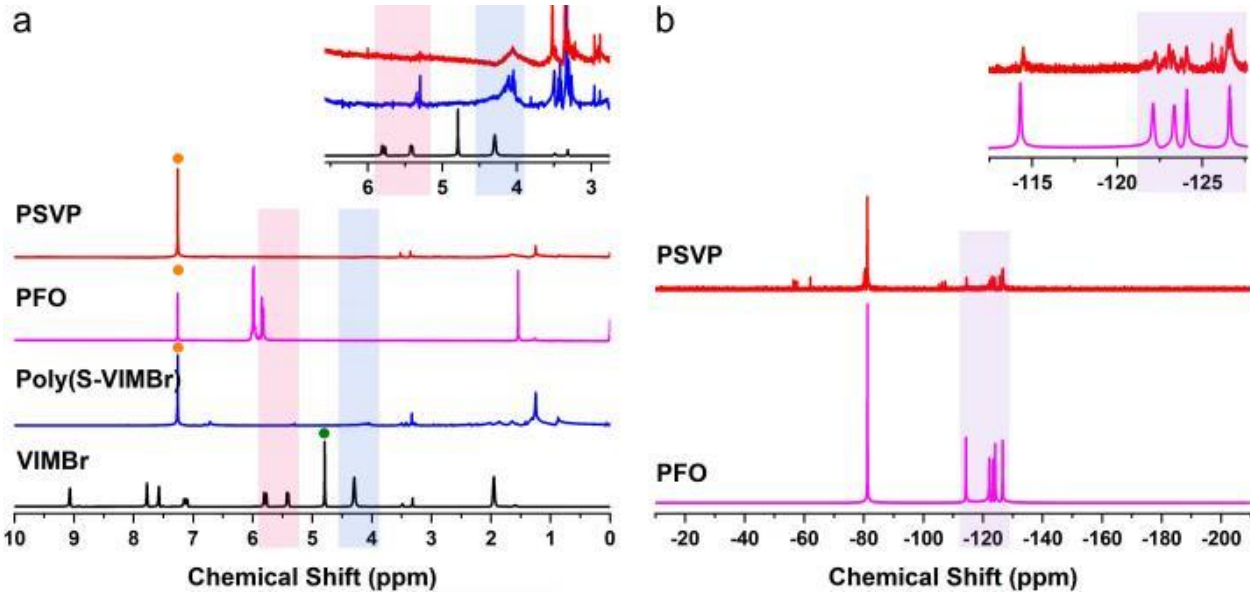

Figure 2. a) ^{1}H NMR spectra of the VIMBr, Poly(S-VIMBr), PFO and PSVP, the illustration is a partial enlarged view of VIMBr, Poly(S-VIMBr) and PSVP, the orange solid circle represents $CDCl_3$, the green solid circle represents D_2O; b) ^{19}F NMR spectra of the PFO and PSVP, illustration is a partial enlarged view of PFO and PSVP.

the peaks of at 5.80 and 5.40 ppm attributed to =C-H and $=CH_2$ of VIMBr mostly disappeared in the spectrum of Poly(S-VIMBr), indicating the conversion of C=C to C-C in VIMBr

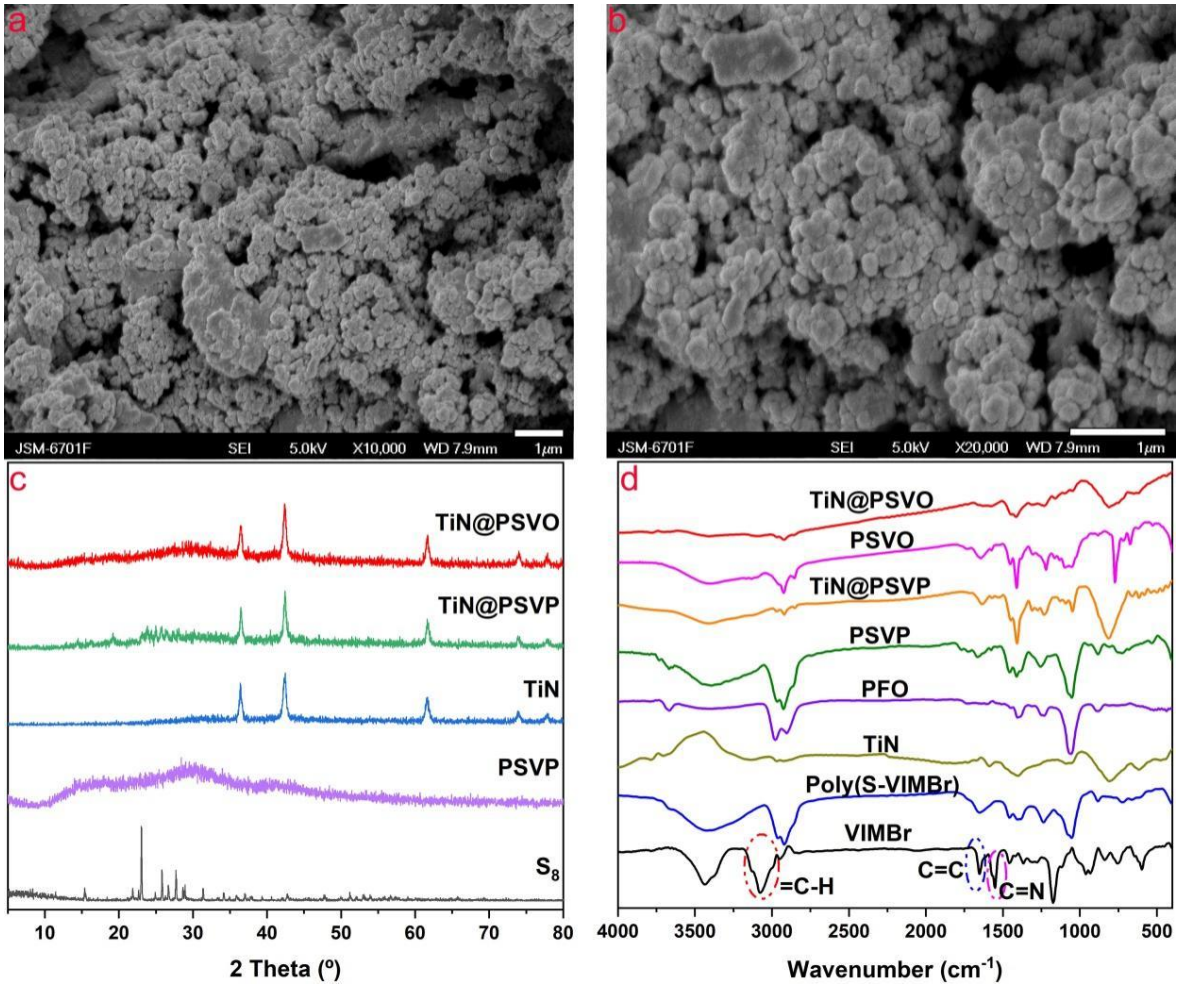

Figure 3. SEM images of TiN@PSVP (a, b); c) PXRD spectra of S8, PSVP, TiN, TiN@PSVP and TiN@PSVO; d) FTIR spectra of VIMBr, Poly(S-VIMBr), TiN, PFO, PSVP, TiN@PSVP and TiN@PSVO.

crosslinkers. Meanwhile, the complete consumption of double bond peaks at 5.98 and 5.82 ppm of PFO in PSVP and the signals at 1 - 3.5 and 3.7 - 4.5 ppm attributed to the alkane proton of -CH_2- and S-C-H proton peaks revealed the presence of PFO in the designed polymers (Figure 2a).[43] The weakened and broaden peaks of ^{19}F NMR of PFO at -130 to -110 ppm in the PSVP exemplified tailed PFO in the designed polymers (Figure 2b), presumably, due to the chemical shifts of multiple fluorine atoms after polymerization. This has also been implicated by the FTIR spectrum (Figure 3d). Thus, compared to the spectrum of the pristine VIMBr, the =C-H and C=C peaks in the 3077 and 1651 cm^{-1} bands of Poly(S-VIMBr) are weakened or faded, revealing reacted double bonds after the IV reaction of S_8 with VIMBr. The peaks of PSVP at 1413, 1235 and 893 cm^{-1} bands originated from the stretching vibration peaks of C-C, -CF_2- and -CF_3 bonds supported that PFO was successfully grafted into the Poly(S-VIMBr).[44-46] The radical scavenger TEMPO or BHT was introduced into the reaction system to disclose that PFO was triggered by the active radicals present in poly(S-VIMBr) (Figure S11).

Morphology and Microstructure of Nanoparticles

The morphology of the samples was characterized by scanning electron microscopy (SEM). As illustrated in Figure 3a and 3b, the surface of TiN@PSVP has grooves with second-order micro-nano roughness, these shapes and structures are conducive to the fine superhydrophobic features of the materials. Compared to PSVP, the corresponding energy-dispersive X-ray spectroscopy (EDS) of TiN@PSVP (Figure S12, S13) shows that the characteristic elements of the material surface include C, N, F, S, Ti and Br atoms. The atomic percentage of N (24.5%) is significantly larger than that of Ti (12.9%), indicating the existence of both TiN and imidazole ionic liquids in the materials, which further proves the generation of PSVP encapsulated TiN nanoparticles.

The powder X-ray diffraction (PXRD) patterns indicated the crystal structures of the as-obtained composite material (Figure 3c). The obvious characteristic diffraction peaks of TiN@PSVP and TiN@PSVO have been seen at 2θ values of 36.4º, 42.4º, 61.6º, 73.9º, and 77.8º, corresponding to TiN itself, and the positions of the diffraction peaks are almost identical.[47] No peaks for crystalline S_8 were observed in the PXRD characterization. However, the crystallization and melting of residual S_8 in the TiN@PSVP composite were observed by DSC (Differential scanning calorimetry, see later - Figure 5b), centering at 24.7 and 111.2 °C.[48] This is probably due to depolymerization from unstable high sulfur rank polysulfide chains, or amorphous S_8 physically trapped within the polymer potentially on the surface of the TiN nanoparticles. In the room temperature PXRD characterization there is therefore no detection, but in DSC the heating step provides sufficient energy for diffusion and crystallization.

The The Fourier transform infrared (FTIR) spectra of TiN@PSVP and TiN@PSVO nanoparticles are shown in Figure 3d. The characteristic peaks of the pristine VIMBr located at 3130, 1551 and 1173 cm^{-1} bands are ascribed to the representative stretching vibrations of C-H, C=N and C-N in the imidazole ring. In addition, the peaks at 3077, 2950 and 1651 cm^{-1} are attributed to the stretching vibration peaks of =CH, -CH_2- and C=C.[44] The peak around 1413 cm^{-1} is the stretching vibration of the C-C bond in the TiN@PSVP and TiN@PSVO, whilst those peaks around 1235 and 893 cm^{-1} belong to -CF_2- and -CF_3 bonds stretching vibration in PFO, PSVP and TiN@PSVP.[44-46] All these data reveals that TiN@PSVP and TiN@PSVO have been constructed successfully (Figure S10).

X-ray photoelectron spectroscopy (XPS) were used to further examine the chemical ingredient and surface states of the PSVP and TiN@PSVP, and illuminated the mechanism of wettability change (Figure 4). The results in Figure 4a imply that the major elemental compositions of PSVP and TiN@PSVP are

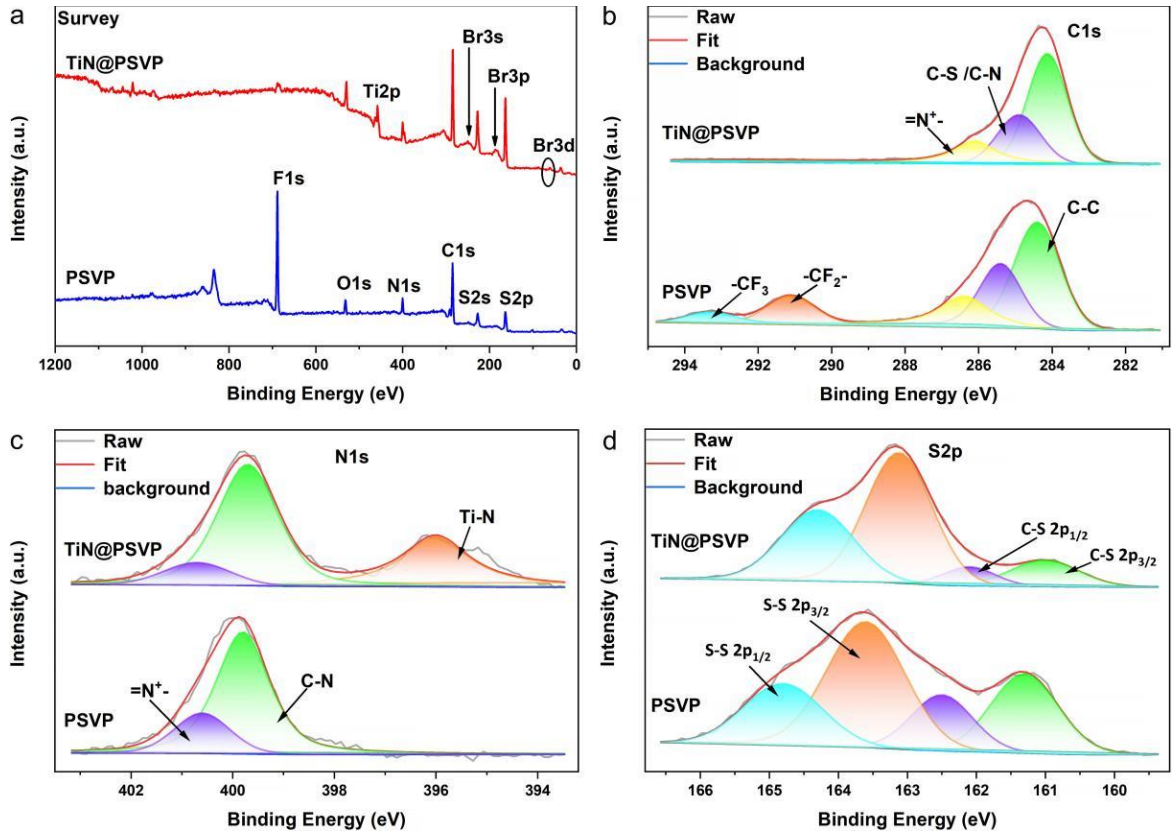

Figure 4. a) XPS survey spectra of PSVP and TiN@PSVP; b) C1s spectra of PSVP and TiN@PSVP; c) N1s spectra of PSVP and TiN@PSVP; c) S2p spectra of PSVP and TiN@PSVP.

different. Compared with PSVP, TiN@PSVP shows a new peak at 457.7 eV representing Ti2p.[47] On the surface of TiN@PSVP, the C1s core-level spectrum may be deconvoluted into five peaks at 284.1, 284.9, 286.1, 290.8 and 293.1 eV (Figure 4b), which represent C-C, C-N/C-S, $=N^{+}$-, $-CF_2$- and $-CF_3$, respectively.[45,47,49-52] It is found that the binding energies of the above elements are shifted after the TiN nanoparticles are introduced. Analogously, Figure 3c shows the N 1s spectrum of PSVP can be deconvoluted into two peaks, which correspond to tertiary nitrogen C-N (399.8 eV) and the ammonium group $=N^{+}$- (400.6 eV) in the imidazole ring, respectively. After compositing with TiN, the peak at 396.0 eV could be attributed to Ti-N,[53,54] indicating that PSVP might encapsulate TiN nanoparticles. Meanwhile, the S2p spectrum (Figure 4d) recognizes that TiN@PSVP can be divided into four peaks at 161.0, 162.1, 163.1 and 164.3 eV, whereas the binding energies of the $S2p_{3/2}$ (161.0 eV) and $S2p_{1/2}$ (162.1 eV) are attributed to C-S bond, and the binding energies of $S2p_{3/2}$ (163.1 eV) and $S2p_{1/2}$ (164.3 eV) are assigned to S-S linkage.[55,56] The existence of C-S and S-S bonds signifies the formation of linear sulfur bridges for the S_8 ring after IV reaction. Compared to PSVP (F=29.02%, at.%), the XPS results are evidenced that the fluorine atoms on the surface of TiN@PSVP nanoparticles are relatively small (4.38 at.%), which is in agreement with the EDS results. A further confirmation is that the low surface energy PFO groups are successfully grafted on the TiN@Poly(S-VIMBr) surface. Thus, the effect of PFO on the wettability of polymer-coated TiN-based materials could be negligible.

Thermal properties of the PSVP and TiN@PSVP were investigate by thermogravimetric analysis (TGA) and DSC under a N_2 atmosphere. Figure 5a shows the 5% thermal decomposition temperature ($T_{deg,5\%}$) of obtained PSVP and TiN@PSVP, is up to about 250 and 200 °C. Subsequently, $T_{deg,5\%}$ of the PSVP and TiN@PSVP are lower than that the corresponding S_8 probably due to the comparatively fragile S-S bonds in the polymers.[56] Continuous weight loss of PSVP is observed after 330 °C, while the weight loss for TiN@PSVP is relatively gentle at similar temperature, indicating that the cross-linked structure has a better stabilizing effect on the nanoparticles. No apparent glass transition temperature (T_g) was obtained for PSVP, so were the TiN@PSVP (Figure 5b). It could be the condition of DSC applied is limited in evaluating the main thermal properties of sulfur-based polymers in PSVP[57] as well as the fact that the segments of the cross-linked structure were immobilized on the TiN nanoparticles surface.[58]

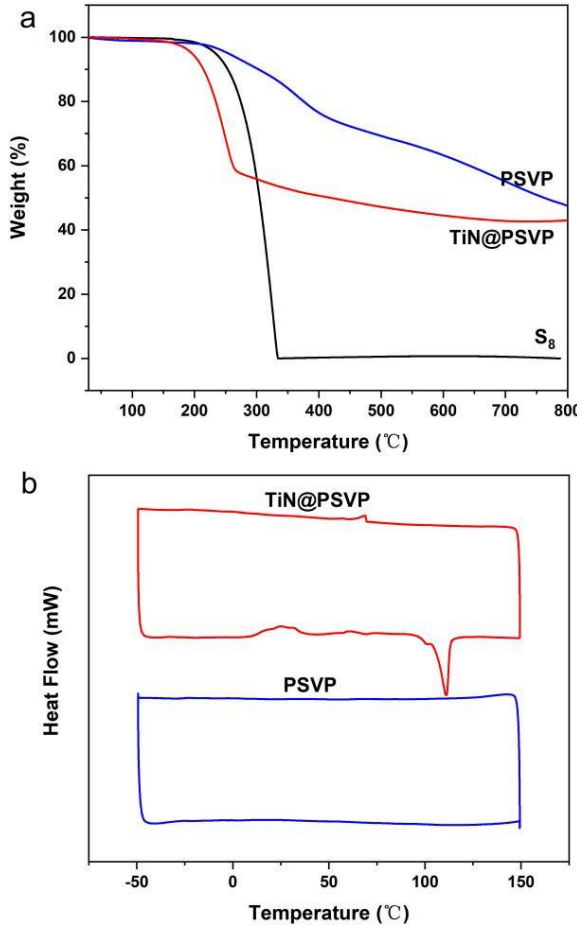

Figure 5. a) TGA thermograms of S_8, PSVP and TiN@PSVP; b) DSC thermograms of PSVP and TiN@PSVP coating.

Contact Angle Measurement

The effect of different TiN ratios on wettability was systematically investigated subsequently. The WCA of the coating gradually increased with the increase of amount of TiN (≦ 60 mg, Figure 6a and Entries 1-3 in Table S1); however, the WCA gradually decreased with further increasement of TiN (up to 100 mg, Entries 3-7 in Table S1). The enhanced micro-nano roughness of the constructed material by the addition of small amount of TiN could increase the WCA dominantly. The existence of excess TiN could generate a large number of microclusters, reducing the compactness and the WCA of the coating. Thus, the optimal amount of TiN is 60 mg regarding the compactness of the coating, and the ratio among S, VIMBr and PFO is 1:1:1, the WCA of TiN@PSVP coating is 162.6 ± 0.4°. Sulfur-rich polymer-modified TiN nanoparticles can further reduce the surface energy and successfully fabricate

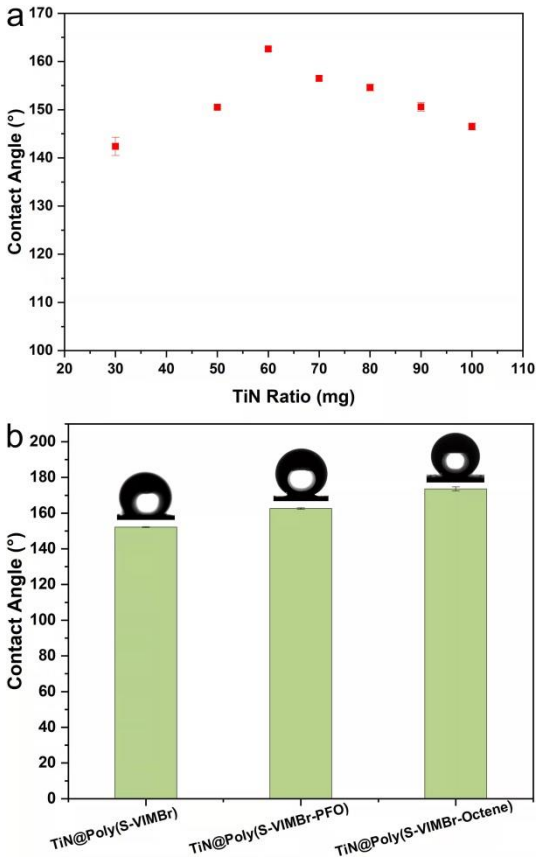

Figure 6. a) Different amounts of TiN affect the WCA of TiN@PSVP coating; b) Variation of WCA after peeling of TiN@PSVP coating.

superhydrophobic coatings on glass substrates. The wettability of different substances coated on TiN nanoparticles shows obvious WCA effect (Table S2), the WCA of TiN@Poly(S-VIMBr) and TiN@PSVO are 152.2 ± 0.2° and 173.6 ± 1.1°, respectively (Figure 6b). It is noteworthy that the low surface energy PFO has little effect on the TiN-based superhydrophobic materials, providing an environmentally friendly fluorine-free superhydrophobic material.

Table 2. Protection efficiency calculated from Tafel curve and equation (1)

Samples	E_{corr} /V	I_{corr}/A cm^{-2}	η /%
Mg	-1.795	1.704×10^{-4}	-
Mg/TiN@Poly(S-VIMBr-PFO)	-1.711	3.682×10^{-6}	97.84
Mg/TiN@Poly(S-DAS-PFO)	-1.364	4.697×10^{-6}	97.24
Mg/TiN@Poly(S-DVB-PFO)	-1.339	1.181×10^{-5}	93.07
Mg/TiN@Poly(S-DIB-PFO)	-1.413	8.178×10^{-6}	95.20
Mg/TiN@Poly(S-VIMBr-Octene)	-1.377	4.485×10^{-6}	97.15
Mg/TiN@Poly(S-DAS-Octene)	-1.357	1.664×10^{-5}	90.23
Mg/TiN@Poly(S-DVB-Octene)	-1.399	1.239×10^{-5}	92.73

Compared to the wettability of the materials obtained with different cross-linking agents, the cross-linking agent VIMBr is the most promising one (Figure 6b, S3). Thus, with the optimal feed of TiN@PSVP, the WCA of TiN@Poly(S-DAS-PFO) reaches 166.8 ± 0.3° with 1,2-diallyldisulfane. Interestingly, with a more rigid crosslinker, Interestingly, with a more rigid crosslinker, DVB or DIB, the WCA can reach up to 157.5 ± 0.9° and 165.4 ± 0.7° with optimized conditions (Table 2, Figure S14). Moreover, the wettability of environmentally benign materials was investigated with the optimal ratio of TiN@PSVP. Thus, the WCA with VIMBr crosslinker can reach 173.6 ± 1.1°. The primary results suggest that a higher WCA achieved with TiN used as the substrate nanoparticle with the ionic liquid as the cross-linkers. Of interesting note is that the long-chain olefins and fluorine-containing olefins have similar effect of constructing superhydrophobicity in this case.

Self-cleaning property of the superhydrophobic surface was assessed by using TiN@PSVP sprayed glass slide with tilting angle. After a small amount of sand was sprinkled on the coating, the surface of the coating becomes clean after washing with dropped water, with no considerable difference from the uncontaminated sample (Video S1).[31] Of note is that the water droplets had a bouncing behavior on the surface of the coating, indicating excellent superhydrophobic and self-cleaning properties of the surface covered by TiN@PSVP. Meanwhile, the mechanical properties of the material were qualitatively tested by peeling experiments, and it was found that the WCA reduced from 162.6±0.4° to 151.3±0.4° with the number of peeling times reached 200 times (Table S3), but the coating remained superhydrophobic.

Corrosion Resistance of the Coating

The Tafel polarization curves of coated Mg alloy substrates tested in NaCl solution (3.5 wt%). As seen in Table 2, the corrosion potential (E_{corr}) and corrosion current density (I_{corr}) tested for bare Mg are -1.795 V and 1.704×10^{-4} A·cm^{-2}, respectively, while the E_{corr} and I_{corr} of the coated Mg sheet (Mg/TiN@PSVO) were -1.377 V and 4.485×10^{-6} A·cm^{-2}, and the E_{corr} and I_{corr} of Mg/TiN@PSVP were -1.711 V and 3.682×10^{-6} A·cm^{-2}, respectively, the decrease of 2 magnitude orders were obtained (Figures S15, S16). The E_{corr} of the superhydrophobic samples shifted in the positive direction by approximately 418 mV and 84 mV. These results indicated that the composite TiN@PSVP and TiN@PSVO coating significantly increased the anti-corrosion of Mg alloy sheets. The corresponding coating protection rate (η) of the TiN@PSVP and TiN@PSVO coating is as high as 97.8% and 97.2% as calculated by equation (1).[59]

$$\eta = \frac{I_{corr0} - I_{corr}}{I_{corr0}} \times 100\% \quad (1)$$

where I_{corr0} and I_{corr} are the current density of bare Mg alloy and coated Mg sheet, respectively. Although the coating protection performance of similar materials obtained with other crosslinkers or octene also exceeded 90% (Figure S15, S16, Table 2), these TiN-embedded materials have excellent anti-corrosion, and the higher the WCA of the coating, the better the protection performance of Mg alloys.

Antibacterial activity

Antibacterial testing of TiN@PSVP was conducted by the plate colony count method (Figure 7). Gram-negative bacteria *E. coli* and Gram-positive bacteria *S. aureus* were proceeded as representative strains. Figure 7A and 7B are strains of *S. aureus* formed on LB agar plates, the blank group was carried out in PBS buffer solution (Figure 7A), compared to the plate containing TiN@PSVP (200 μg/mL) composite (Fig. 7B), the number of colonies changed significantly, and the inhibitive rate of TiN@PSVP against *S. aureus* was calculated to be 79.9%

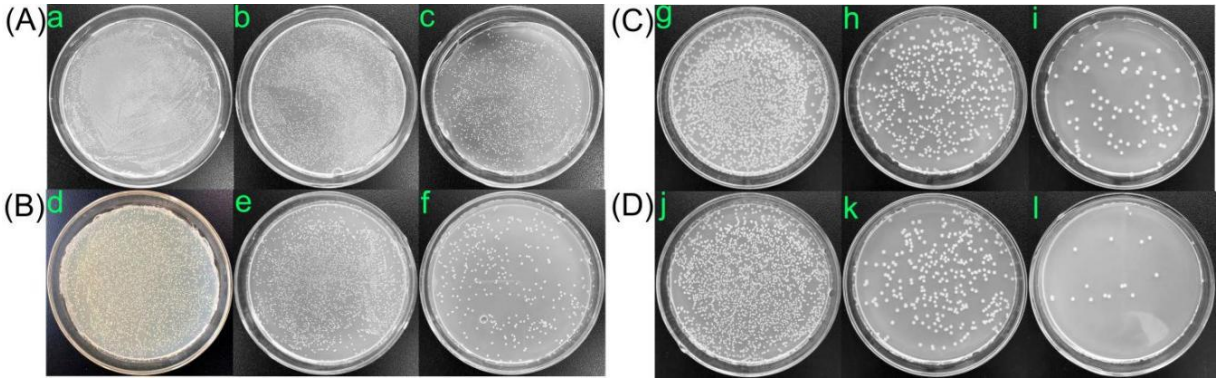

Figure 7. Representative colonies of *S. aureus* formed on LB agar plates in the presence of (A) PBS solution and (B) TiN@PSVP, a-c and d-f were serial 10-fold dilutions; Representative colonies of *E. coli* formed on LB agar plates in the presence of (C) PBS solution and (D) TiN@PSVP, and g-i and j-l were serial 10-fold dilutions.

(Table S4). Representative strains of *E. coli* formed on LB agar plates are shown in Figures 7C and 7D. Compared with the blank control (Figure 7C), the number of colonies on the plate containing TiN@PSVP composite (Figure 7C) changed significantly, the calculated inhibitive rate of TiN@PSVP against *E. coli* was 66.1% (Table S4). The antibacterial effects of fluorine-free TiN@PSVO materials against *S. aureus* and *E. coli* are shown in Figure S17. The inhibitive rate of TiN@PSVO against *S. aureus* and *E. coli* were calculated to be 92.9% and 63.3% (Table S5).

4 Conclusions

In summary, a facile approach to fabricate TiN-loaded sulfur-rich polymers by IV reaction was demonstrated, revealing the superhydrophobicity, anti-corrosion and antibacterial properties of the prepared composites. The micro-structures and thermal properties of the TiN@PSVP and TiN@PSVO coating were characterized, the hierarchical micro- and nanostructures improved the superhydrophobicity of the material. The TiN@PSVO material has good to excellent properties of superhydrophobicity (WCA of 173.6 ± 1.1°), the WCA of TiN@Poly(S-VIMBr) and TiN@Poly(S-VIMBr-PFO) coatings are 152.2 ± 0.2° and 162.6 ± 0.4°, respectively. Meanwhile, the protection efficiency up to 97.2% for Mg in 3.5% NaCl is achieved, and the composites obtained with ionic liquid crosslinkers exhibited higher WCA and coating protection ratios. The antibacterial activity experiment shows activity against both *E. coli* and *S. aureus* with inhibitive rates of 63.3% and 92.9%, respectively. Replacing the fluorine-containing olefins with environmentally benign and low-cost long-chain olefins achieved similar or even better effect of building superhydrophobic properties, avoiding the large-scale usage of fluorine-containing olefins for coating materials as non-toxic beneficial to both humans and environment with broaden practical application potential.

Acknowledgement

The authors thank the National Nature Science Foundation of China (22067018, 22101232) and Natural Science Foundation of Gansu Province (20YF3GA023) for financial support. Thanks also to the Programme of Introducing Talents of Discipline to Universities (No. B16017). Y. P., S.C., H.W., and X.D. thank the China Scholarship Council for studentship assistance. T.H. thanks the Royal Society University Research Fellowship. The water contact angle test was assisted by Prof Li Jian and his research group. Antibacterial experiments were performed at the College of Life Sciences, Northwest Normal University. The authors are also very appreciated to the Materials Innovation Factory (MIF) team members in the University of Liverpool for their assistance in operating the instruments.

References

1. T Lee, P. T. Dirlam, J. T. Njardarson, R. S. Glass, J. Pyun, *J. Am. Chem. Soc.* **2022**, *144*, 5.
2. W. J. Chung, J. J. Griebel, E. T. Kim, H. Yoon, A. G. Simmonds, H. J. Ji, P. T. Dirlam,R. S. Glass, J. J. Wie, N. A. Nguyen, B. W. Guralnick, J. Park, A. Somogyi, P. Theato, M. E. Mackay, Y. E. Sung, K. Char, J. Pyun, *Nat. Chem.* **2013**, *5*, 518.
3. K. W. Park, E. M. Leitao, *Chem. Commun.* **2021**, *57*, 3190.
4. Y. Zhang, R. S. Glass, K. Char, J. Pyun, *Polym. Chem.* **2019**, *10*, 4078.
5. M. J. H. Worthington, R. L. Kucera, J. M. Chalker, *Green Chem.* **2017**, *19*, 2748.
6. X. F. Wu, J. A. Smith, S. Petcher, B. W. Zhang, D. J. Parker, G. M. Griffin, T. Hasell, *Nat. Commun.* **2019**, *10*, 647.
7. L. J. Dodd, O. Omar, X. F. Wu, T. Hasell, *ACS Catal.* **2021**, *11*, 4441.
8. J. M. Chalker, M. J. H. Worthington, N. A. Lundquist, L. J. Esdaile, *Top. Curr. Chem.* **2019**, *377*, 16.
9. I. Gomez, D. Mecerreyes, J. A. Blazquez, O. Leonet, H. B. Youcef, C. M. Li,J. L. Gomez-Camer, O. Bundarchuk, L. Rodriguez-Martinez, *J. Power Sources* **2016**, *329*, 72.
10. G. Gao, X. Sun, L. Wang, *J. Mater. Chem. A* **2020**, *8*, 21711.
11. H. Kang, H. Kim, M. J. Park, *Adv. Energy Mater.* **2018**, *8*, 1802423.
12. D. J. Parker, H. A. Jones, S. Petcher, L. Cervini, J. M. Griffin, R. Akhtar, T. Hasell, *J. Mater. Chem. A* **2017**, *5*, 11682.
13. M. J. H. Worthington, R. L. Kucera, I. S. Albuquerque, C. T. Gibson, A. Sibley, A. D. Slattery, J. A. Campbell,; Alboaiji, S. F. K.; Muller, K. A.; Young, J.; Adamson, N.; Gascooke, J. R.; Jampaiah, D.; Sabri, Y. M.; Bhargava, S. K.; Ippolito, S. J.; Lewis, D. A.; Quinton, J. S.; Ellis, A. V.; Johs, A.; Bernardes, G. J. L.; Chalker, J. M. *Chem. Eur. J.* **2017**, *23*, 16219.
14. T. Hasell, D. J. Parker, H. A. Jones, T. McAllister, S. M. Howdle, *Chem. Commun.* **2016**, *52*, 5383.
15. M. P. Crockett, A. M. Evans, M. J. H. Worthington, I. S. Albuquerque, A. D. Slattery, C. T. Gibson, J. A. Campbell, D. A. Lewis, G. J. L. Bernardes, J. M. Chalker, *Angew. Chem. Int. Ed.* **2016**, *55*, 1714.
16. J. M. Chalker, M. Manna,M. J. H. Worthingtona, L. J. Esdaile, *Org. Mater.* **2021**, *3*, 362.
17. J. J. Griebel, S. Namnabat, E. T. Kim, R. Himmelhuber, D. H. Moronta, W. J. Chung, A. G. Simmonds, K. J. Kim, J. Laan, N. A. Nguyen, E. L. Dereniak, M. E. Mackay, K. Char, R. S. Glass, R. A. Norwood, J. Pyun, *Adv. Mater.* **2014**, *26*, 3014.
18. T. S. Kleine, R. S. Glass, D. L. Lichtenberger, M. E. Mackay, K. Char, R. A. Norwood, J. Pyun, *ACS Macro Lett.* **2020**, *9*, 245.
19. M. Mann, J. E. Kruger, F. Andari, J. McErlean, J. R. Gascooke, J. A. Smith, M. J. H. Worthington, C. C. C. McKinley, J. A. Campbell, D. A. Lewis, T. Hasell, M. V. Perkins, J. M. Chalker, *Org. Biomol. Chem.* **2019**, *17*, 1929.
20. S. F. Valle, A. S. Giroto, R. Klaic, G. G. F. Guimaraes, C. Ribeiro, *Polym. Degrad. Stabil.* **2019**, *162*, 102.
21. J. A. Smith, R. Mulhall, S. Goodman, G. Fleming, H. Allison, R. Raval, T. Hasell, *ACS Omega* **2020**, *5*, 5229.
22. Z. L. Deng, A. Hoefling, P. Théato, K. Lienkamp, *Macromol. Chem. Phys.* **2018**, *219*, 1700497.
23. R. A. Dop, D. R. Neill, T. Hasell, *Biomacromolecules* **2021**, *22*, 5223.
24. T. Thiounn, A. G. Tennyson, R. C. Smith, *RSC Adv.* **2019**, *9*, 31460.
25. C. V. Lopez, M. S. Karunarathna, M. K. Lauer, C. P. Maladeniya, T. Thiounn, E. D. Ackley, R. C. Smith, *J. Polym. Sci.* **2020**, *58*, 2259.
26. M. Mann, B. Zhang, S. J. Tonkin, C. T. Gibson, Z. Jia, T. Hasell, J. M. Chalker, *Polym. Chem.* **2022**, *13*, 1320.
27. C. Peng, Z. Chen, M. K. Tiwari, *Nat. Mater.* **2018**, *17*, 355.
28. D. E. Weibel, A. F. Michels, A. F. Feil, L. Amaral, S. R. Teixeira, F. Horowitz, *J. Phys. Chem. C* **2010**, *114*, 13219.
29. T. He, Y. Wang, Y. Zhang, Q. Lv, T. Xu, T. Liu, *Corros. Sci.* **2009**, *51*, 1757.
30. Y. Liu, H. Cao, S. Chen, D. Wang, *J. Phys. Chem. C* **2015**, *119*, 25449.
31. W. Cao, Y. Liu, M. Ma, J. Zhu, *Colloids Surf. A Physicochem. Eng. Aspects* **2017**, *529*, 18.
32. C. Xia, Y. Li, T. Fei, W. Gong, *Chem. Eng. J.* **2018**, *345*,

648.
33. Y. Huang, Y. Shan, S. Liang, X. Zhao, G. Jiang, C. Hu, J. Yang, L. Liu, *J. Mater. Chem. A* **2018**, *6*, 17156.
34. Y. Song, Y. Liu, H. Jiang, S. Li, C. Kaya, T. Stegmaier, Z. Han, L. Ren, *Nanoscale* **2018**, *10*, 3813.
35. H. Xu, S. Fan, Y. Lu, H. Feng, J. Qiu, *Bull. Chem. Soc. Jpn.* **2020**, *93*, 91114.
36. H. Xu, Y. Wang, D. Zhao, N. Chen, L. Tan, H. Feng et al, *Bull. Chem. Soc. Jpn.* **2021**, *94*, 2390.
37. J. Zhi, L. Zhang, Y. Yan, J. Zhu, *Appl. Surf. Sci.* **2017**, *392*, 286.
38. Z. He, M. Ma, X. Lan, F. Chen, K. Wang, H. Deng, Q. Zhang, Q. Fu, *Soft Matter* **2011**, *7*, 6435.
39. D. Goswami, S. K. Medda, G. De, *ACS Appl. Mater. Interfaces* **2011**, *3*, 3440.
40. M. Choi, Y. Kim, S. Park, D. Ka, T. Kim, S. Lee, E. H. Sohn, Y. Jin, J. Hong, *Adv. Funct. Mater.* **2021**, *31*, 2101511.
41. C. Miao, X. Xun, L. J. Dodd, S Niu, H Wang, P Yan, X. Wang, J. Li, X. Wu, T. Hasell, Z.n Quan, *ACS Appl. Polym. Mater.* **2022**, 10.1021/acsapm.2c00490.
42. C. Miao, F. Li, Y. Zuo, R. Wang, Y. Xiong, *RSC Adv.* **2016**, *6*, 3013.
43. Y. Wei, X. Li, Z. Xu, H. Sun, Y. Zheng, L. Peng, Z. Liu, C. Gao, M. Gao, *Polym. Chem.* **2015**, *6*, 9.
44. C. Mu, J. Ren, H. Chen, Y. Wu, Q. Xu, X. Sun, K. Yan, *ACS Appl. Nano Mater.* **2021**, *4*, 10634.
45. Z. Chen, J. Droste, G. Zhai, J. Zhu, J. Yang, M. R. Hansen, X. Zhuang, *Chem. Commun.* **2019**, *55*, 9047.
46. Y. Xu, M. Li, M. Liu, *Prog. Org. Coat.* **2019**, *134*, 177.
47. X. Tian, J. Luo, H. Nan, Z. Fu, J. Zeng, S. Liao, *J. Mater. Chem. A*, **2015**, *3*, 16801.
48. M. Arslan, B. Kiskan, Y. Yagci, *Macromolecules* **2016**, *49*, 767.
49. J. Chen, Y. Cheng, Q. Zhang, C. Luo, H. Li, Y. Wu, H. Zhang, X. Wang, H. Liu, X. He, J. Han, D. Peng, M. Liu, M. Wang, *Adv. Funct. Mater.* **2021**, *31*, 2007158.
50. S. Zeng, L. Li, L. Xie, D. Zhao, N. Wang, S. Chen, *Chemsuschem* **2017**, *10*, 3378.
51. J. Peng, S. Yuan, H. Geng, X. Zhang, M. Zhang, F. Xu, D. Lin, Y. Gao, H. Wang, *Chem. Eng. J.* **2022**, *428*, 131162.
52. Y. Charles-Blin, D. Flahaut, J. Ledeuil, K. Guérin, M. Dubois, M. Deschamps, A. Perbost, L. Monconduit, H. Martinez, N. Louvain, *ACS Appl. Energy Mater.* **2019**, *2*, 6681.
53. J. Liu, Y. Zhu, X. Chen, W. Yi, *J. Alloys Compd.* **2020**, *815*, 152328.
54. X. Tian, H. Tang, J. Luo, H. Nan, T. Shu, L. Du, J. Zeng, S. Liao, R. R. Adzic, *ACS Catal.* **2017**, *7*, 3810.
55. H, Kim, J. Lee, H. Ahn, O. Kim, M. J. Park, *Nat. Commun.* **2015**, *6*, 7278.
56. X Liu, Y Lu, Q Zeng, P. Chen, Z. Li, X. Wen, W. Wen, Z. Li, L. Zhang, *ChemSusChem* **2020**, *13*, 715.
57. A. S. M. Ghumman, M. M. Nasef, M. R. Shamsuddin, A. Abbasi, *Polym. Polym. Compos.* **2021**, *29*, 1333.
58. J. Ma, J. Fan, S. Chen, X. Yang, K. N. Hui, H. Zhang, C. W. Bielawski, J. Geng, *ACS Appl. Mater. Interfaces* **2019**, *11*, 13234.
59. D. Li, H. Wang, Y. Liu, D. Wei, Z. Zhao, *Chem. Eng. J.* **2019**, *367*, 169.

Graphical Abstract

<Title>

Fabrication of TiN-based Superhydrophobic Anti-corrosion Coating by Inverse Vulcanization

<Authors' names>

Congcong Miao,[1] Peiyao Yan,[2] Haichao Liu,[1] Shanshan (Diana) Cai,[2] Liam J. Dodd,[2] Haoran Wang,[2] Xi Deng,[2] Jian Li,[1] Xi-Cun Wang,[1] Xiaolin Hu,[3] Xiaofeng Wu,[1,2*] Tom Hasell,[1,2*] Zheng-Jun Quan[1*]

<Summary>

The synthesis of TiN-embedded sulfur-rich polymer micro-nanoparticles by inverse vulcanization reaction revealed the superhydrophobicity, corrosion resistance and antibacterial properties of the resultant composites, with WCA of the coating up to 173.6 ± 1.1°. This protocol provides a feasible method for the preparation of eco-friendly and environmentally benign fluorine-free superhydrophobic anti-corrosion materials in practical applications.

Length of summary should be about 50-60 words.